Journal of Neuroscience Methods 343 (2020) 108840

Contents lists available at ScienceDirect

Journal of Neuroscience Methods

journal homepage: www.elsevier.com/locate/jneumeth

Invited review

AIMAFE: Autism spectrum disorder identification with multi-atlas deep feature representation and ensemble learning

Yufei Wang[a], Jianxin Wang[a], Fang-Xiang Wu[b], Rahmatjan Hayrat[a], Jin Liu[a,*]

[a] Hunan Provincial Key Lab on Bioinformatics, School of Computer Science and Engineering, Central South University, Changsha 410083, China
[b] Division of Biomedical Engineering and Department of Mechanical Engineering, University of Saskatchewan, Saskatoon S7N 5A9, Canada

ARTICLE INFO

Keywords:
Autism spectrum disorder identification
Functional magnetic resonance imaging
Functional connectivity
Stacked denoising autoencoder
Ensemble learning

ABSTRACT

Background: Autism spectrum disorder (ASD) is a neurodevelopmental disorder that could cause problems in social communications. Clinically, diagnosing ASD mainly relies on behavioral criteria while this approach is not objective enough and could cause delayed diagnosis. Since functional magnetic resonance imaging (fMRI) can measure brain activity, it provides data for the study of brain dysfunction disorders and has been widely used in ASD identification. However, satisfactory accuracy for ASD identification has not been achieved.

New method: To improve the performance of ASD identification, we propose an ASD identification method based on multi-atlas deep feature representation and ensemble learning. We first calculate multiple functional connectivity based on different brain atlases from fMRI data of each subject. Then, to get the more discriminative features for ASD identification, we propose a multi-atlas deep feature representation method based on stacked denoising autoencoder (SDA). Finally, we propose multilayer perceptron (MLP) and an ensemble learning method to perform the final ASD identification task.

Results: Our proposed method is evaluated on 949 subjects (including 419 ASDs and 530 typical control (TCs)) from the Autism Brain Imaging Data Exchange (ABIDE) and achieves accuracy of 74.52% (sensitivity of 80.69%, specificity of 66.71%, AUC of 0.8026) for ASD identification.

Comparison with existing methods: Compared with some previously published methods, our proposed method obtains the better performance for ASD identification.

Conclusion: The results suggest that our proposed method is efficient to improve the performance of ASD identification, and is promising for ASD clinical diagnosis.

1. Introduction

Autism spectrum disorder (ASD) (Amaral et al., 2008) is a neurodevelopmental disorder that affects social interaction and communication (Kim et al., 2011). Families of patients with ASD face a non-negligible economic burden (Ou et al., 2015). The clinical diagnosis of ASD based on behavioral criteria, assessed using tools such as the autism diagnostic observation schedule (ADOS) (Lord et al., 2000) and autism diagnostic interview-revised (ADI-R) (Lord et al., 1994), has been criticized as lacking objectivity (Timimi et al., 2019) and being likely to lead to misdiagnosis or delayed diagnosis (Wang et al., 2017b). In addition, clinical diagnosis of ASD relies on professional doctors which consumes a lot of medical resources. Thus, it is appealing to develop a more convenient and objective diagnostic method to identify ASD (Yerys and Pennington, 2011).

Currently, magnetic resonance imaging (MRI) has provided a way for clinicians to understand the pathophysiology of brain disorders, such as schizophrenia (Liu et al., 2017, 2018d), ASD (Kong et al., 2019; Wang et al., 2017a) and Alzheimer's disease (Liu et al., 2018b,c). MRI is an imaging technology that can recognize brain disorders based on brain structure. MRI is also a low-cost and non-invasive diagnostic tool which has been widely used in medical field. Specifically, since functional MRI (fMRI) (Huettel et al., 2004; Fox and Raichle, 2007; Buxton, 2009) can infer brain activity by measuring blood oxygen level signals over time, it has attracted increasing attention from researchers engaged in brain dysfunction research (Iidaka, 2015; Dvornek et al., 2017; Liu et al., 2020; Xiang et al., 2020). Brain activity is quantified by changes in the intensity of fMRI images during the acquisition time, which is usually represented by a time series. In general, brain disorders are not just abnormalities in one or several brain regions, but an

* Corresponding author.
E-mail addresses: willem@csu.edu.cn (Y. Wang), jxwang@mail.csu.edu.cn (J. Wang), faw341@mail.usask.ca (F.-X. Wu), rahmatjan@csu.edu.cn (R. Hayrat), liujin06@csu.edu.cn (J. Liu).

https://doi.org/10.1016/j.jneumeth.2020.108840
Received 12 December 2019; Received in revised form 30 June 2020; Accepted 30 June 2020
Available online 09 July 2020

abnormal connectivity between brain regions. Therefore, to explore the correlation of certain activities between brain regions, functional connectivity (FC) has been proposed and is widely used for the classification and prediction of brain disorders (Du et al., 2018).

In the past decade, some researchers have combined FC and machine learning methods (such as support vector machines (SVMs)) to classify patients with ASD from typical controls (TCs) based on fMRI data (Plitt et al., 2015; Anderson et al., 2011; Chen et al., 2016; Jahedi et al., 2017; Abraham et al., 2017). For example, Chen et al. (2016) first calculated two FCs based on the Dosenbach atlas (Dosenbach et al., 2010) and two frequency bands: slow-4 frequencies (0.027–0.073 Hz) and slow-5 frequencies (0.01–0.027 Hz) which were proposed by Zuo et al. (2010), and then combined the top ranked features of these two FCs via *F*-scores to perform ASD classification. Jahedi et al. (2017) first extracted FC based on the brain atlas proposed by Power et al. (2011) as the original features of each subject, and then used a conditional random forest (CRF)-based dimension reduction algorithm to obtain more discriminative features to perform ASD classification. Abraham et al. (2017) first extracted a group brain atlas based on a multisubject dictionary learning (MSDL) algorithm, and then calculated the FC based on the group brain atlas using a tangent space embedding algorithm to obtain the features for ASD classification. In recent years, deep learning methods (LeCun et al., 2015) have shown great potential in many areas, including medical image analysis (Litjens et al., 2017; Liu et al., 2018a). Compared with traditional machine learning methods, deep learning methods can automatically learn more hidden features from raw data with multilayer neural networks. For example, Heinsfeld et al. (2018) proposed an ASD identification method that used a stacked denoising autoencoder (SDA) (Vincent et al., 2010) for pretraining to learn a deep feature representation from FC based on the Craddock 200 (CC200) (Craddock et al., 2012) atlas. Parisot et al. (2018) first calculated FC based on the Harvard-Oxford atlas as the original features of each subject, and then used graph convolutional networks (GCNs) to learn the deep feature representation from the FC of each subject to perform ASD classification. Table 1 summarizes some existing FC-based ASD identification methods. To date, although some FC-based studies have obtained relatively good ASD identification results, satisfactory results have not been obtained in clinical practice. Therefore, this is still a challenging problem for ASD identification.

To address this challenging problem, in this study we propose an improved ASD identification method using multi-atlas deep feature representation and ensemble learning which we term “Autism spectrum disorder Identification with Multi-Atlas deep Feature representation and Ensemble learning (AIMAFE)”. First, we calculate three FCs between the time series of brain regions based on three different brain atlases. Then, to obtain a more discriminative feature representation for ASD identification, we propose a multi-atlas deep feature representation method based on an SDA. Finally, we propose a multilayer perceptron (MLP) and an ensemble learning method to combine multiple deep feature representations to perform the final ASD identification task. Our proposed method is evaluated on the Autism Brain Imaging Data Exchange (ABIDE) dataset.

2. Methods

The architecture of our proposed method for identifying subjects with ASD and TCs is shown in Fig. 1. As shown in Fig. 1, our proposed method consists of three main parts: data preprocessing and functional connectivity, multi-atlas deep feature representation, and classification. We first compute the FC between each pair of regions based on three different brain atlases from fMRI data of each subject, and extract these FCs as the original features. After this step, we can obtain three feature representations. Then, to obtain more effective features for ASD/TC classification, we apply the SDA to perform the multi-atlas deep feature representation. Finally, we propose a MLP and an ensemble learning method to perform the final ASD identification task.

2.1. Data preprocessing and functional connectivity

In this study, the experimental data come from the Autism Brain Imaging Data Exchange (ABIDE) dataset. The ABIDE consists of 17 international acquisition sites and the data vary across sites. The data preprocessing is based on the preprocessed fMRI datasets using the Configurable Pipeline for the Analysis of Connectomes (CPAC) (Craddock et al., 2013) from the Preprocessed Connectomes Project. More detailed information about the data is available at http://preprocessed-connectomes-project.org/. For the preprocessed fMRI data downloaded from http://preprocessed-connectomes-project.org/abide/, we found some subjects who had missing time-series. Therefore, in this study we excluded all subjects who had missing time-series as data quality control. Through data quality control, we selected 419 subjects with ASD and 530 TC subjects as experimental subjects in this study. The demographic information of the experimental subjects in this study is summarized in Table 2.

As shown in Fig. 1, we next calculate FC based on three brain atlases (i.e., CC200, AAL (Automated Anatomical Labeling (Tzourio-Mazoyer et al., 2002)) and Dosenbach) as the original feature representation of each subject. In this study, the weights of the FC are calculated by Pearson correlation coefficient (PCC) between the time series of each pair of brain regions from the same brain atlas, as follows:

$$\mathrm{PCC}(r_i, r_j) = \frac{E(r_i r_j) - E(r_i)E(r_j)}{\sqrt{E(r_i^2) - E^2(r_i)}\sqrt{E(r_j^2) - E^2(r_j)}} \quad (1)$$

where r_i and r_j denote the time series of brain regions i and j, respectively, and $E(\cdot)$ denotes the mathematical expectation. Taking the AAL atlas as an example, for each subject, we first calculate the PCC of the time series between the paired brain regions from the AAL atlas and obtain a 116×116 symmetric matrix, and then take the lower triangle of the symmetric matrix as the original feature representation of this subject. The calculation procedure of the other two atlases (i.e., CC200 and Dosenbach) is similar to that of AAL.

Through the above calculation procedure, for each subject, we obtain three original FC feature representations based on the above three atlases, which are denoted as F_{CC}, F_{AAL}, and F_{DOH}. These three FC feature representation are used as input for the next step as shown in Fig. 1.

2.2. Multi-atlas deep feature representation

To achieve more discriminative features from F_{CC}, F_{AAL}, and F_{DOH} for ASD identification, we propose a multi-atlas deep feature

Table 1
Summary of some existing FC-based ASD identification methods.

References	Number (ASD/TC)	Original features	Dimension reduction	Classifier
Chen et al. (2016)	112/128	FC	*F*-score	SVM
Jahedi et al. (2017)	126/126	FC	CRF	RF
Abraham et al. (2017)	403/468	FC	–	SVM
Heinsfeld et al. (2018)	505/530	FC	SDA	Softmax
Parisot et al. (2018)	403/468	FC	GCN	Softmax

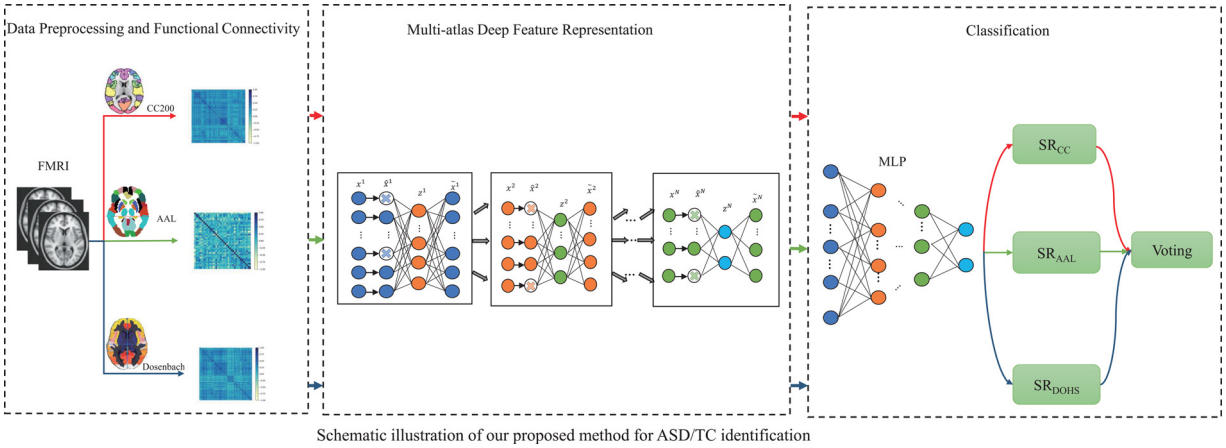

Fig. 1. Schematic illustration of our proposed method for ASD/TC identification.

Table 2
Demographic information for the subjects in this study.

Site	ASD/TC	Age mean(STD)	Male/female	Time-series
CALTECH	14/18	27.36(10.62)	25/7	146
CMU	13/13	26.69(5.77)	20/6	236/316
KKI	18/28	10.02(1.25)	34/12	152
LEUVEN	20/34	17.81(4.74)	46/8	246
MAX MUN	17/28	25.42(11.13)	42/3	116/196
NYU	60/100	15.51(6.66)	125/35	176
OHSU	9/14	10.87(1.80)	23/0	78
OLIN	18/15	16.67(3.49)	29/4	206
PITT	24/27	18.89(6.91)	45/6	196
SBL	12/15	32.85(6.14)	27/0	196
SDSU	9/22	14.32(1.88)	24/7	176
STANFORD	17/20	9.89(1.59)	30/7	176
TRINITY	19/25	16.90(3.49)	44/0	146
UCLA	46/44	12.90(2.12)	79/11	116
UM	58/74	14.09(3.25)	106/26	296
USM	42/25	22.74(8.57)	67/0	236
YALE	23/28	12.79(2.89)	37/14	196
Total	419/530	16.88(7.76)	803/146	–

representation method based on SDA which is shown in Fig. 1.

A denoising autoencoder (DAE) (Vincent et al., 2008) as a feed-forward neural network is usually used for feature selection, feature dimensionality reduction and unsupervised feature self-learning in which the raw vectors at the input layer are reconstructed at the output layer by an intermediate layer with a reduced number of hidden nodes. A DAE can learn high-order and abstract features from corrupted data with noise. The noise in the DAE is obtained by randomly transforming some values in the FC matrix to zero according to binomial distributions in the training data. The noise in the DAE is added according to a percentage C. The DAE focuses on minimizing the reconstruction loss between the raw data and the corrupted version of the data. The corrupted input data decrease the generation gap between the training data and test data to a certain extent. In this case, the DAE will find stable and useful features that constitute an advanced description of the input data. In addition, to avoid the over-learning in the network, we add the Kullback–Leibler (KL) divergence to limit the activation of hidden nodes. The cost function of the DAE is as follows:

$$J_{\mathrm{DAE}} = \sum_{i=1}^{m} \frac{1}{2} \parallel x^i - g(f(\hat{x}^i)) \parallel^2 + \beta \sum_{j=1}^{s} \mathrm{KL}(\rho||\hat{\rho}_j) \tag{2}$$

$$\mathrm{KL}(\rho||\hat{\rho}_j) = \rho \log \frac{\rho}{\hat{\rho}_j} + (1-\rho)\log \frac{1-\rho}{1-\hat{\rho}_j} \tag{3}$$

$$\hat{\rho}_j = \frac{1}{m} \sum_{i=1}^{m} a_j^2(x^i) \tag{4}$$

where m is the number of input training subjects, x^i is the ith input data value, $\hat{x}^i$ is the corrupted ith input data value, $f(\cdot)$ is the encoding function, $g(\cdot)$ is the decoding function, $\mathrm{KL}(\rho||\hat{\rho}_j)$ is a sparse penalty term, ρ is a sparse parameter, s is the number of hidden nodes, $\hat{\rho}$ is the average activation, $a_j^2(x^i)$ is the output of the jth neuron, and β is the sparse penalty.

When faced with complicated learning problems, the learning ability of a single DAE is limited. Therefore, a stacked denoising auto-encoder (SDA) (Vincent et al., 2010) is proposed to address the problem. The SDA is a stack of N DAEs. The input of each DAE is the output of the preceding DAE's hidden layer. For example, as Fig. 1 shows, z^1 is the output of the first DAE's hidden layer. x^2 is the input of the second DAE, and z^1 is equal to x^2. The SDA learns features with a greedy layerwise training method that is conducted on the unlabeled training dataset. However, the input of the first DAE is the high-dimensional raw data, and the large number of hidden nodes is not conducive to obtaining a deep feature representation of the input. Therefore, KL divergence is added in the first DAE. With the DAEs stacked, the number of hidden nodes decreases, the DAEs become increasingly simplified, and KL divergence is prevented, which starts with the second DAE.

2.3. Classification

As seen in Fig. 1, the classification part of our proposed method includes two steps: a MLP with a softmax regression method and a voting strategy.

Step 1: The weights from multiple hidden layers of the SDA are applied as the initial weights of the MLP. We use the labeled dataset to perform supervised learning. The parameters of all layers are optimized by error back propagation, and then the parameters are updated to minimize the training error. The inputs of the MLP are the feature representation obtained from data preprocessing and the functional connectivity. The outputs of the MLP are two units that represent the probability of the label of each subject.

The F_{AAL} feature representation is obtained after performing data preprocessing and obtaining the functional connectivity. Then we use the SDA which is a stack of N DAEs to perform unsupervised learning and the MLP to perform supervised learning based on F_{AAL}. We obtain a deep feature representation (F_{AALS}). The process of obtaining deep feature representations of the other two feature representations (F_{CC} and F_{DOH}) is similar to that used for F_{AAL}. After this step, we obtain three deep feature representations (denoted as F_{AALS}, F_{CCS} and F_{DOHS}).

Then we use a softmax regression method (LeCun et al., 2015) to calculate probabilities to determine the label of each subject. The inputs of the softmax regression (i.e., SR_{AAL}, SR_{CC} and SR_{DOHS}) are F_{AALS}, F_{CCS} and F_{DOHS}, respectively. The softmax regression method is defined as follows:

$$h_\theta(x) = \frac{1}{\sum_{k=1}^{K} e^{\theta_k^T x}} \begin{bmatrix} e^{\theta_1^T x} \\ e^{\theta_2^T x} \\ \vdots \\ e^{\theta_K^T x} \end{bmatrix} \tag{5}$$

where x, K, θ_k and $h_\theta(x)$ refer to the input data of the subject, the number of labels, the model parameters and the classification probability, respectively. After this step, we obtain the three single classification results of each subject based on the feature representation (denoted as R_{AALS}, R_{CCS} and R_{DOHS}).

Step 2: To fully take advantage of the complementary information among multi-atlas feature representations, we apply an ensemble learning method to integrate all the classification results of each subject. For a subject, the predicted label is the majority of the labels predicted by each individual result of feature representation. If there is a situation in which a subject cannot be classified when we combine two results of a single feature representation, the predicted label for that particular subject is the label that represents the maximum probability of these results for the subject.

3. Experiments and results

3.1. Experimental settings

To obtain an unbiased and robust performance for ASD identification, in this study we adopt a 10-fold cross validation strategy and repeat five experiments. Furthermore, in order to quantify the performance of ASD identification, in this study we calculate the average values in five 10-fold cross-validation experiments for the three metrics of accuracy (ACC), sensitivity (SEN), and specificity (SPE), which are formulated as follows:

$$\mathrm{ACC} = \frac{1}{5}\sum_{i=1}^{5} \frac{\mathrm{TP}_i + \mathrm{TN}_i}{\mathrm{TP}_i + \mathrm{TN}_i + \mathrm{FP}_i + \mathrm{FN}_i} \tag{6}$$

$$\mathrm{SEN} = \frac{1}{5}\sum_{i=1}^{5} \frac{\mathrm{TP}_i}{\mathrm{TP}_i + \mathrm{FN}_i} \tag{7}$$

$$\mathrm{SPE} = \frac{1}{5}\sum_{i=1}^{5} \frac{\mathrm{TN}_i}{\mathrm{TN}_i + \mathrm{FP}_i} \tag{8}$$

where TP_i, FP_i, TN_i and FN_i are the number of correctly classified positive subjects, the number of incorrectly classified positive subjects, the number of correctly classified negative subjects, and the number of incorrectly classified negative subjects in the ith experiment, respectively. In addition, we also calculate the area under the receiver operating characteristic curve (AUC) to evaluate the overall performance of our proposed method for ASD identification.

The parameters in our proposed framework are set as follows: number of DAEs N: 3; data corruption of DAEs C: {30%, 10% and 10%}; sparse parameter: 0.2; number of hidden layers: 3; number of hidden layer nodes: 2500, 1250, 625; learning rate: 0.0005; activation function: tanh; sparse penalty β: 0.5. For more details on the parameter settings, please see https://github.com/wyf1995/AIMAFE.

3.2. Experimental results

In this study, we first perform ASD identification based on the single-atlas deep feature representation (i.e., F_{CCS}, F_{AALS} and F_{DOHS}) in the proposed framework, and then perform ASD identification based on multi-atlas deep feature representation in the proposed framework. For ASD identification experiments based on multi-atlas deep feature representation in the proposed framework, we adopt a progressive strategy to avoid useless combinations. The specific procedure is to first use the best ASD identification accuracy obtained from a single-atlas deep feature representation as the basis, and then use our proposed voting method to gradually integrate the next best ASD identification accuracy obtained by a single-atlas deep feature representation to obtain the final ASD identification accuracy. Table 3 shows the ASD identification performance of the proposed framework using different numbers of deep feature representations.

Table 3
The ASD identification performance of the proposed framework using different numbers of deep feature representations.

Feature representation	ACC (%)	SEN (%)	SPE (%)	AUC	p-value
F_{CCS}	73.39	79.58	65.56	0.8002	0.02
F_{AALS}	71.42	78.98	61.85	0.7835	< 0.01
F_{DOHS}	69.74	77.25	60.25	0.7685	< 0.01
$F_{CCS} + F_{AALS}$	73.60	80.45	64.94	0.7993	0.03
$F_{CCS} + F_{AALS} + F_{DOHS}$	74.52	80.69	66.71	0.8026	

As seen from Table 3, the single-atlas deep feature representation: F_{CCS} achieves better ASD identification performance (including better ACC, SEN and SPE values) than the other two single-atlas deep feature representations (i.e., F_{AALS} and F_{DOHS}) in the proposed framework. Furthermore, with the increasing number of deep feature representations in the proposed framework, the ASD identification performance improves, and finally the best ASD identification performance (i.e., ACC: 74.52%, SEN: 80.69% and SPE: 66.71%) is obtained by using three deep feature representations (i.e., $F_{CCS} + F_{AALS} + F_{DOHS}$). These results show that our proposed method (i.e., AIMAFE) is effective for ASD identification. In addition, we also observe that the AUC value of our proposed method is greater than 0.8. The result shows that our proposed method is robust to some extent for ASD identification.

To investigate whether there are significant advantages of using three feature representations compared with using any other number of feature representations in the proposed framework for ASD identification, we use a two sample t-test method to calculate the difference (i.e., p-value) between them based on the ACC, as shown in Table 3. As seen from Table 3, all p-values are less than 0.05. The results show that there are significant advantages of using three feature representations compared to using any other number of feature representations in the proposed framework, and further prove that our proposed method is effective and has certain advantages for ASD identification.

4. Discussion

4.1. Effect of different depths

In this section, to determine how many layers are appropriate for ASD identification, we present the results of different parameters for the number of layers and nodes in a single feature representation. To date, there is no standard principle for selecting the size of the hidden layers and nodes of neural networks. Too many layers and nodes increases the computational resources and cause overfitting. However, too few layers and nodes causes underfitting. Thus, we adopt a progressive strategy to find the best parameters. The numbers of hidden layers and nodes are progressively decreased to find the best parameters. The number of hidden layers ranges from 2 to 5. The number of nodes in the first hidden layer can be set to 5000, 2500, or 1250. The number of nodes decreases by half layer by layer in each experiment. The noise proportion of the corrupted data C is set as {30%, 10%, 10%, …}. For example, when the number of hidden layers is 4 and the number of nodes in the first hidden layer is 5000, the numbers of nodes in the other three hidden layers are set as 2500, 1250 and 625. The proportions of corruption data in the 4 DAEs are set as {30%, 10%, 10%, 10%}. All experimental results are shown in Fig. 2.

As Fig. 2 shows, when the number of hidden layers is 3 and the numbers of hidden nodes are 2500, 1250 and 625, the performance of ASD identification improves. From the results in Fig. 2, the ACCs of R_{DOHS}, R_{AALS} and R_{CCS} are 69.74%, 71.42% and 73.39%, respectively. In

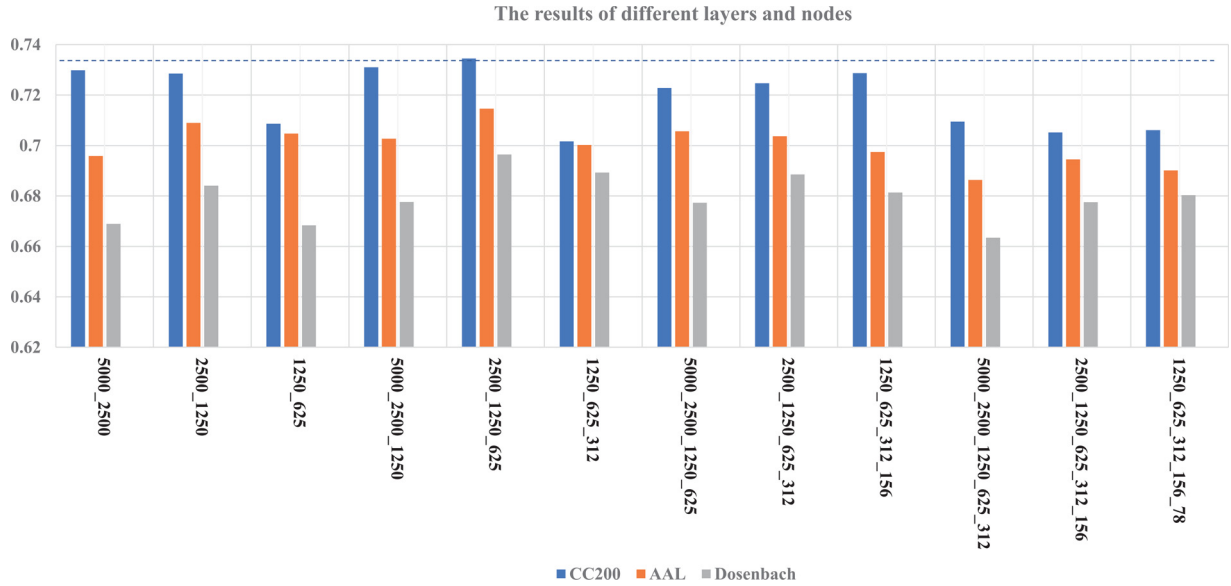

Fig. 2. The accuracy of different parameters of hidden layers and hidden nodes.

summary, these findings of better parameters are meaningful for ASD identification.

4.2. Comparison with different machine learning methods

In this subsection, to demonstrate the superiority of the combination of deep feature representations and softmax regression in our proposed framework for ASD identification, we compare several typical machine learning methods including the linear support vector machine (L-SVM), the radial basis function support vector machine (RBF-SVM), the K-nearest neighbors (KNN) and the random forest (RF). In the specific experimental procedures, the L-SVM is taken as an example. The three connectivity feature representations (i.e., F_{CC}, F_{AAL}, and F_{DOH}) are used as the input of the L-SVM, and then the voting strategy we proposed is used to integrate the output of these three L-SVM as the final ASD identification performance. The experimental procedures of the other three methods (i.e., RBF-SVM, KNN and RF) are similar to that of L-SVM. It is worth mentioning that the four machine learning methods are performed with the Scikit-learn library (Pedregosa et al., 2011), and each machine learning method uses the default parameters of the Scikit-learn library. In addition, we also use the two sample *t*-test method to evaluate the differences between our proposed method and the other machine learning methods based on the ACC. The comparative results are shown in Table 4.

As seen from Table 4, the method combining deep feature representation and softmax regression method that we propose achieves the best ACC, SEN, SPE and AUC values for ASD identification. The comparative results indicate that our proposed method is effective and superior for ASD identification. In addition, we also observe that all $p-$values are less than 0.01. The difference analysis results further show that our proposed method has significant advantages.

4.3. Comparison with existing methods

In this subsection, to verify the superiority of our proposed method, we compare some existing FC-based ASD identification methods as shown in Table 1. The experimental results of these comparative methods are briefly described as follows: Chen et al. (2016) achieved an accuracy of 74% when using both slow-4 and slow-5 features. However, when using only slow-4 or slow-5 features, we could only obtain an accuracy of 69%. Abraham et al. (2017) separately used six brain atlases for ASD classification with SVM as a classifier. The best results were provided using the multi-subject dictionary learning atlas (MSDL), which achieved an accuracy of 66.8%. Jahedi et al. (2017) used FC based on the power brain atlas (Power et al., 2011) and a conditional random forest as a classifier for ASD classification which achieves an accuracy of 66.7%. Parisot et al. (2018) used the Harvard-Oxford atlas to extract FC as features, and then they used graph convolutional networks to obtain 2000 low-dimensional features for classification which achieved an accuracy of 70.4%. Heinsfeld et al. (2018) proposed a method that used two SDAs and a neural network for ASD classification based on the CC200 brain atlas which achieved an accuracy of 70%. They also used the Dosenbach and AAL atlases separately to classify ASD reaching a lower accuracy.

The comparative experimental results are shown in Table 5. Our results are close to those of Chen et al. (2016), but Chen et al. (2016) used only ASD adolescents from the ABIDE database. Therefore, since our experimental data include more subjects in different age groups, our results are more comprehensive, indicating the robustness of our method. Compared with Jahedi et al. (2017) and Parisot et al. (2018), we fully use multi-atlas information to improve the ASD identification performance. In addition, although Abraham et al. (2017) and Heinsfeld et al. (2018) used more than one atlas, they did not combine

Table 4
Comparison with different machine learning methods.

Method	ACC (%)	SEN (%)	SPE (%)	AUC	*p*-value
L-SVM	66.79	67.82	65.52	0.7217	< 0.01
RBF-SVM	68.73	69.18	68.28	0.7556	< 0.01
KNN	63.61	71.50	53.46	0.6573	< 0.01
RF	67.87	78.30	54.20	0.7392	< 0.01
Our proposal	74.52	80.69	66.71	0.8026	

Table 5
Comparison with existing methods.

Methods	ACC (%)
Chen et al. (2016)	74.00
Jahedi et al. (2017)	66.70
Abraham et al. (2017)	66.80
Heinsfeld et al. (2018)	70.00
Parisot et al. (2018)	70.40
AIMAFE	74.52

the results from the various atlases, ignoring the complementary information which might be present in different atlases. We combine the results of different feature representations based on different atlases which achieves a higher accuracy. In summary, our proposed method is effective for ASD identification.

4.4. Limitations

In the present study, we obtain a better performance for identifying ASD with our proposed method than other methods achieve. However, there are some limitations of our proposed method. First, our proposed method is only tested on the ABIDE dataset which is not very robust. Second, demographic information is not considered in this paper. There is increasing evidence that ASD is related to sex and age (Werling and Geschwind, 2013; Kana et al., 2014). For example, males are more susceptible than females. Third, we only used fMRI data in this study. However, different image modalities (such as structural MRI (sMRI) and positron emission tomography (PET), etc.) may contain complementary information for ASD identification. Therefore, we will try to address these limitations as much as possible in future work regarding ASD identification.

5. Conclusions

In this study, we propose an automatic ASD identification method based on multi-atlas deep feature representation and ensemble learning using fMRI data. Experimental results on the ABIDE dataset demonstrate the effectiveness of the proposed method in ASD identification task. This method paves the way for discriminative image markers for the automatic diagnosis of ASD. In addition, compared with some state-of-the-art methods, our proposed method obtains the best accuracy and has certain advantages for ASD identification, indicating that this method is promising for the automatic diagnosis of ASD in clinical practice.

Authors' contribution

Yufei Wang: conceptualization, methodology, software, writing – reviewing and editing. Jianxin Wang: methodology, writing – reviewing and editing. Fang-Xiang Wu: methodology. Rahmatjan Hayrat: methodology. Jin Liu: conceptualization, methodology, writing – reviewing and editing

Conflict of interest

None declared.

Acknowledgements

This work is supported in part by the National Natural Science Foundation of China under Grant Nos. 61802442,61702122, the Natural Science Foundation of Hunan Province under Grant Nos. 2019JJ50775,2018JJ2534, the 111 Project (No. B18059), the Hunan Provincial Science and Technology Program (2018WK4001), the Fundamental Research Funds for the Central Universities of Central South University (2019zzts590).

References

Abraham, A., Milham, M.P., Di Martino, A., Craddock, R.C., Samaras, D., Thirion, B., Varoquaux, G., 2017. Deriving reproducible biomarkers from multi-site resting-state data: an autism-based example. NeuroImage 147, 736–745.

Amaral, D.G., Schumann, C.M., Nordahl, C.W., 2008. Neuroanatomy of autism. Trends Neurosci. 31 (3), 137–145.

Anderson, J.S., Nielsen, J.A., Froehlich, A.L., DuBray, M.B., Druzgal, T.J., Cariello, A.N., Cooperrider, J.R., Zielinski, B.A., Ravichandran, C., Fletcher, P.T., et al., 2011. Functional connectivity magnetic resonance imaging classification of autism. Brain 134 (12), 3742–3754.

Buxton, R.B., 2009. Introduction to Functional Magnetic Resonance Imaging: Principles and Techniques. Cambridge University Press.

Chen, H., Duan, X., Liu, F., Lu, F., Ma, X., Zhang, Y., Uddin, L.Q., Chen, H., 2016. Multivariate classification of autism spectrum disorder using frequency-specific resting-state functional connectivity – a multi-center study. Prog. Neuro-Psychopharmacol. Biol. Psychiatry 64, 1–9.

Craddock, R.C., James, G.A., Holtzheimer III, P.E., Hu, X.P., Mayberg, H.S., 2012. A whole brain fMRI atlas generated via spatially constrained spectral clustering. Human Brain Mapp. 33 (8), 1914–1928.

Craddock, C., Sikka, S., Cheung, B., Khanuja, R., Ghosh, S.S., Yan, C., Li, Q., Lurie, D., Vogelstein, J., Burns, R., et al., 2013. Towards automated analysis of connectomes: the configurable pipeline for the analysis of connectomes (c-pac). Front. Neuroinform. 42.

Dosenbach, N.U., Nardos, B., Cohen, A.L., Fair, D.A., Power, J.D., Church, J.A., Nelson, S.M., Wig, G.S., Vogel, A.C., Lessov-Schlaggar, C.N., et al., 2010. Prediction of individual brain maturity using fMRI. Science 329 (5997), 1358–1361.

Du, Y., Fu, Z., Calhoun, V.D., 2018. Classification and prediction of brain disorders using functional connectivity: promising but challenging. Front. Neurosci. 12, 525.

Dvornek, N.C., Ventola, P., Pelphrey, K.A., Duncan, J.S., 2017. Identifying autism from resting-state fMRI using long short-term memory networks. International Workshop on Machine Learning in Medical Imaging 362–370.

Fox, M.D., Raichle, M.E., 2007. Spontaneous fluctuations in brain activity observed with functional magnetic resonance imaging. Nat. Rev. Neurosci. 8 (9), 700–711.

Heinsfeld, A.S., Franco, A.R., Craddock, R.C., Buchweitz, A., Meneguzzi, F., 2018. Identification of autism spectrum disorder using deep learning and the abide dataset. NeuroImage: Clin. 17, 16–23.

Huettel, S.A., Song, A.W., McCarthy, G., et al., 2004. Functional Magnetic Resonance Imaging, vol. 1. Sinauer Associates, Sunderland, MA.

Iidaka, T., 2015. Resting state functional magnetic resonance imaging and neural network classified autism and control. Cortex 63, 55–67.

Jahedi, A., Nasamran, C.A., Faires, B., Fan, J., Müller, R.-A., 2017. Distributed intrinsic functional connectivity patterns predict diagnostic status in large autism cohort. Brain Connect. 7 (8), 515–525.

Kana, R.K., Uddin, L.Q., Kenet, T., Chugani, D., Müller, R.-A., 2014. Brain connectivity in autism. Front. Human Neurosci. 8, 349.

Kim, Y.S., Leventhal, B.L., Koh, Y.-J., Fombonne, E., Laska, E., Lim, E.-C., Cheon, K.-A., Kim, S.-J., Kim, Y.-K., Lee, H., et al., 2011. Prevalence of autism spectrum disorders in a total population sample. Am. J. Psychiatry 168 (9), 904–912.

Kong, Y., Gao, J., Xu, Y., Pan, Y., Wang, J., Liu, J., 2019. Classification of autism spectrum disorder by combining brain connectivity and deep neural network classifier. Neurocomputing 324, 63–68.

LeCun, Y., Bengio, Y., Hinton, G., 2015. Deep learning. Nature 521 (7553), 436–444.

Litjens, G., Kooi, T., Bejnordi, B.E., Setio, A.A.A., Ciompi, F., Ghafoorian, M., Van Der Laak, J.A., Van Ginneken, B., Sánchez, C.I., 2017. A survey on deep learning in medical image analysis. Med. Image Anal. 42, 60–88.

Liu, J., Li, M., Pan, Y., Wu, F.-X., Chen, X., Wang, J., 2017. Classification of schizophrenia based on individual hierarchical brain networks constructed from structural MRI images. IEEE Trans. Nanobiosci. 16 (7), 600–608.

Liu, J., Pan, Y., Li, M., Chen, Z., Tang, L., Lu, C., Wang, J., 2018a. Applications of deep learning to MRI images: a survey. Big Data Mining Anal. 1 (1), 1–18.

Liu, J., Li, M., Lan, W., Wu, F.-X., Pan, Y., Wang, J., 2018b. Classification of Alzheimer's disease using whole brain hierarchical network. IEEE/ACM Trans. Comput. Bio. Bioinformatics 15 (2), 624–632.

Liu, J., Wang, J., Tang, Z., Hu, B., Wu, F.-X., Pan, Y., 2018c. Improving Alzheimer's disease classification by combining multiple measures. IEEE/ACM Trans. Comput. Biol. Bioinformatics 15 (5), 1649–1659.

Liu, J., Wang, X., Zhang, X., Pan, Y., Wang, X., Wang, J., 2018d. MMM: classification of schizophrenia using multi-modality multi-atlas feature representation and multi-kernel learning. Multimedia Tools Appl. 77 (22), 29651–29667.

Liu, J., Pan, Y., Wu, F.-X., Wang, J., 2020. Enhancing the feature representation of multi-modal MRI data by combining multi-view information for mci classification. Neurocomputing. https://doi.org/10.1016/j.neucom.2020.03.006.

Lord, C., Rutter, M., Le Couteur, A., 1994. Autism diagnostic interview-revised: a revised version of a diagnostic interview for caregivers of individuals with possible pervasive developmental disorders. J. Autism Dev. Disord. 24 (5), 659–685.

Lord, C., Risi, S., Lambrecht, L., Cook, E.H., Leventhal, B.L., DiLavore, P.C., Pickles, A., Rutter, M., 2000. The autism diagnostic observation schedule-generic: a standard measure of social and communication deficits associated with the spectrum of autism. J. Autism Dev. Disord. 30 (3), 205–223.

Ou, J.-J., Shi, L.-J., Xun, G.-L., Chen, C., Wu, R.-R., Luo, X.-R., Zhang, F.-Y., Zhao, J.-P., 2015. Employment and financial burden of families with preschool children diagnosed with autism spectrum disorders in urban china: results from a descriptive study. BMC Psychiatry 15 (1), 3.

Parisot, S., Ktena, S.I., Ferrante, E., Lee, M., Guerrero, R., Glocker, B., Rueckert, D., 2018. Disease prediction using graph convolutional networks: application to autism spectrum disorder and Alzheimer's disease. Med. Image Anal. 48, 117–130.

Pedregosa, F., Varoquaux, G., Gramfort, A., Michel, V., Thirion, B., Grisel, O., Blondel, M., Prettenhofer, P., Weiss, R., Dubourg, V., Vanderplas, J., Passos, A., Cournapeau, D., Brucher, M., Perrot, M., Duchesnay, E., Scikit-learn:, 2011. Machine learning in Python. J. Mach. Learn. Res. 12, 2825–2830.

Plitt, M., Barnes, K.A., Martin, A., 2015. Functional connectivity classification of autism identifies highly predictive brain features but falls short of biomarker standards. NeuroImage: Clin. 7, 359–366.

Power, J.D., Cohen, A.L., Nelson, S.M., Wig, G.S., Barnes, K.A., Church, J.A., Vogel, A.C., Laumann, T.O., Miezin, F.M., Schlaggar, B.L., et al., 2011. Functional network

organization of the human brain. Neuron 72 (4), 665–678.
Timimi, S., Milton, D., Bovell, V., Kapp, S., Russell, G., 2019. Deconstructing diagnosis: four commentaries on a diagnostic tool to assess individuals for autism spectrum disorders. Autonomy (Birm) 1 (6), 1–39.
Tzourio-Mazoyer, N., Landeau, B., Papathanassiou, D., Crivello, F., Etard, O., Delcroix, N., Mazoyer, B., Joliot, M., 2002. Automated anatomical labeling of activations in SPM using a macroscopic anatomical parcellation of the MNI MRI single-subject brain. Neuroimage 15 (1), 273–289.
Vincent, P., Larochelle, H., Bengio, Y., Manzagol, P.-A., 2008. Extracting and composing robust features with denoising autoencoders. Proceedings of the 25th International Conference on Machine Learning 1096–1103.
Vincent, P., Larochelle, H., Lajoie, I., Bengio, Y., Manzagol, P.-A., 2010. Stacked denoising autoencoders: learning useful representations in a deep network with a local denoising criterion. J. Mach. Learn. Res. 11 (Dec), 3371–3408.
Wang, J., Wang, Q., Peng, J., Nie, D., Zhao, F., Kim, M., Zhang, H., Wee, C.-Y., Wang, S., Shen, D., 2017a. Multi-task diagnosis for autism spectrum disorders using multi-modality features: a multi-center study. Human Brain Mapp. 38 (6), 3081–3097.
Wang, S., Deng, H., You, C., Chen, K., Li, J., Tang, C., Ceng, C., Zou, Y., Zou, X., 2017b. Sex differences in diagnosis and clinical phenotypes of Chinese children with autism spectrum disorder. Neurosci. Bull. 33 (2), 153–160.
Werling, D.M., Geschwind, D.H., 2013. Sex differences in autism spectrum disorders. Curr. Opin. Neurol. 26 (2), 146.
Xiang, Y., Wang, J., Tan, G., Wu, F.-X., Liu, J., 2020. Schizophrenia identification using multi-view graph measures of functional brain networks. Front. Bioeng. Biotechnol. 7, 479.
Yerys, B.E., Pennington, B.F., 2011. How do we establish a biological marker for a behaviorally defined disorder?. autism as a test case. Autism Res. 4 (4), 239–241.
Zuo, X.-N., Di Martino, A., Kelly, C., Shehzad, Z.E., Gee, D.G., Klein, D.F., Castellanos, F.X., Biswal, B.B., Milham, M.P., 2010. The oscillating brain: complex and reliable. Neuroimage 49 (2), 1432–1445.